DATA ANALYTICS AND APPLIED MATHEMATICS
E-ISSN: 2773-4854
VOLUME 5, ISSUE 1, 2024, 9 – 18
DOI: https://doi.org/10.15282/daam.v5i1.10348

RESEARCH ARTICLE

Dual slip effects on mixed convective MHD flow with viscous dissipation and Joule heating past an unsteady exponentially stretching sheet

Md. Aminul Islam* and Romena Akter

Department of Natural Sciences, Port City International University, Chattogram, 4217, Bangladesh

ABSTRACT - This study aims to conduct a quantitative examination of the dynamic behaviour of a two-dimensional mixed convection unsteady flow with magnetohydrodynamics (MHD) effects over an exponentially stretching sheet submerged in a permeable medium. In addition to the temperature and velocity slip conditions at the boundary, the study takes into account a number of other variables, including suction or blowing effects, viscous dissipation, heat production or absorption, Joule heating, and thermal radiation. The first step in solving this intricate issue is to apply the necessary similarity transformation to convert the controlling partial differential equations into a set of linked nonlinear ordinary differential equations (ODEs). Subsequently, numerical techniques implemented in MATLAB, particularly employing the bvp4c solver, are utilized to solve the reduced equations. This approach facilitates the exploration of the system's behaviour under different parameter regimes, shedding light on the underlying physical phenomena. The study utilizes both graphs and tables to examine how different parameters affect temperature, velocity, skin-friction coefficients, and Nusselt numbers. Increasing the velocity slip parameter slows down heat transfer and raises skin-friction coefficients, while higher thermal slip parameters reduce heat transmission rates.

ARTICLE HISTORY
Received : 1st Dec 2023
Revised : 18th Feb 2024
Accepted : 17th Mac 2024
Published : 31st Mac 2024

KEYWORDS
Mixed convection
Slip boundary conditions
Joule heating
Viscous dissipation
Thermal radiation

1. INTRODUCTION

Mixed convection flows occur when forced convection is combined with natural convection. This combination is often necessary in high-power devices where forced convection alone cannot provide sufficient cooling. In such cases, adding natural convection helps achieve the desired thermal management. Examples of engineering applications that utilize mixed convection include solar collectors, cooling nuclear reactors during emergency shutdowns, electronic devices cooled by fans, and heat exchangers in low-velocity environments [1-2]. Rehman and Salleh [3] derived an analytic solution for the problem of unsteady mixed convective non-Newtonian hybrid nanofluid flow over a stretching surface by employing the optimal homotopy analysis method. In a different study, Kanafiah et al. [4] investigated how the Brinkman factor influences mixed convective flow around a cylinder-shaped circular. Their findings revealed that an increase in the Brinkman factor guides to a diminution in fluid velocity. Meanwhile, Yahaya et al. [5] investigated unsteady mixed convective hybrid nanofluid with thermal radiation and found that an increase in the unsteadiness parameter led to a reduction in both the velocity profile and the skin friction coefficient.

Radiation is a fundamental procedure where power is released starting a surface as electromagnetic waves in all directions. This phenomenon plays a vital role in engineering and physics, particularly in applications requiring high temperatures, such as nuclear power plants, gas turbines, aircraft, spacecraft, and satellites. Thermal radiation is essential for understanding heat transfer and fluid flow in various technical context [6]. Researchers must address real-world challenges, including chemical processes in fluids that generate or absorb heat. Modelling internal heat generation or absorption can be complex, but simplified mathematical models capture its average behaviour across many physical scenarios. These models provide valuable insights into the impacts of heat creation or absorption, aiding in the understanding and analysis of various phenomena in fluid dynamics and heat transfer [7]. Ishak [8] analysed the steady two-dimensional boundary layer flow and heat transfer over an exponentially stretching sheet (ESS), incorporating the effects of thermal radiation. Sharma and Gupta [9] provided an analytical solution for MHD flow over an ESS, including thermal radiation effects. Omar et al. [10] studied how thermal radiation influences mixed convective flow in Casson fluids.

The Eckert number, which quantifies viscous dissipation, represents the conversion of kinetic energy from fluid motion into thermal and acoustic energy [11]. This dissipation, when multiplied by the magnetic parameter, results in Joule heating, which is crucial for numerous applications such as electric heating devices and electronic equipment [12]. Alinejad et al. [13] investigated how viscous dissipation affects viscous fluid flow past a nonlinearly stretching sheet. Dessie et al. [14] examined its impact on MHD fluid flow through a porous stretching sheet. Patil et al. [15] explored non-similar solutions for double diffusive mixed convection flows over a vertical ESS with viscous dissipation. Shahzad

***CORRESPONDING AUTHOR** | Md. Aminul Islam| ✉ aminulislampciu88@gmail.com

et al. [16] carried out numerical simulations of MHD flow of a Jeffrey nanofluid over a stretching sheet, incorporating Joule heating and viscous dissipation. Mohamed et al. [17] analysed the behaviour of hybrid nanofluids with respect to viscous dissipation.

Velocity slip describes the phenomenon where a fluid does not fully adhere to a solid boundary, which becomes important in scenarios involving polymer solutions and emulsions, where the conventional no-slip state fails. For example, Teflon coatings, known for their slip properties, prevent sticking and are used to polish surfaces like artificial heart valves and internal cavities [18]. The techniques of suction and blowing play a crucial role in various engineering applications, including radial diffusers, the design of thrust bearings, and thermal oil recovery systems [19]. Ramzan et al. [20] analysed the impact of double slip conditions on the flow of mixed convective hybrid nanofluids over a stretching sheet. Islam et al. [21] performed a numerical investigation into how multiple slip conditions influence unsteady MHD flow over an ESS. Furthermore, Islam et al. [22] explored how slip effects affect MHD mixed convective unsteady flow over an ESS. Additionally, Akter and Islam [23] studied the effects of a non-uniform heat source or sink on unsteady MHD Williamson fluid flow over an ESS.

Building on the ideas and practical applications discussed, this study aims to expand upon Mukhopadhyay's work [24] by incorporating additional factors such as porous media, Joule heating, heat generation/absorption, and viscous dissipation into the analysis of MHD unsteady mixed convective flow over an ESS. This study also includes the effects of suction and slip boundary conditions. The dimensionless governing equations are solved numerically using the bvp4c function within the MATLAB. The results are presented for various physical parameters to illustrate their effects.

2. FORMULATION OF THE PROBLEM

Consider MHD boundary layer unsteady flow which is two dimensional, laminar and incompressible over a sheet that stretches exponentially. This sheet is situated within a porous medium. The flow is set up so that the y-axis is perpendicular to the direction of stretching and the x-axis runs parallel to the surface in that direction The stretching surface has the velocity $U(x,t) = \frac{U_0}{1-\alpha t}\, e^{\frac{x}{L}}$ and the temperature distribution $T_w = T_\infty + \frac{T_0}{(1-\alpha t)^2} e^{\frac{x}{2L}}$, where $U_0\,, \alpha,\ L, T_\infty$ and T_0 reference velocity, temperature far away from the stretching surface with $T_w > T_\infty$ and reference temperature respectively. Also applied perpendicular to the sheet is $B(t)$, which represents a changing magnetic field. This magnetic field is described by the expression $B(t) = B_0 e^{x/2L}(1-\alpha t)^{-1/2}$, where B_0 is a constant. The stretching sheet induces a flow in the x -direction, with the flow velocity influenced by the exponential stretching rate of the sheet as a function of x. The governing equations are considered as:

$$u_x + v_y = 0 \tag{1}$$

$$u_t + uu_x + vu_y = \nu u_{yy} + g\beta\,(T - T_\infty) - \frac{\sigma B^2}{\rho} u - \frac{\nu}{K_1}\, u \tag{2}$$

$$\rho\, C_p\,\left(T_t + uT_x + vT_y \right) = \kappa T_{yy} - \frac{\partial q_r}{\partial y} + \sigma B^2 u^2 + \mu\,\left(u_y\right)^2 + Q_0 (T - T_\infty) \tag{3}$$

The associate boundary conditions are

$$\begin{gathered} u = U(x,t) + N\nu\,\frac{\partial u}{\partial y}\ ,\quad V = -V(x,t), T = T_w(x,t) + E\,\frac{\partial T}{\partial y}\quad , at\ y = 0 \\ u \to 0, \qquad T \to T_\infty, \quad as\ y \to \infty \end{gathered} \tag{4}$$

where t is the time, T represents temperature, Q_0 and q_r are the heat generation co-efficient and radiative heat flux, electric conductivity is denoted by σ, μ and ρ represent dynamic viscosity and density respectively, $\nu\ (= \mu/\rho)$ is the kinematic fluid viscosity, κ is the thermal conductivity, C_p is the specific heat at constant pressure, u is the velocity components along the x axis, v is the velocity components along the y axis, g is the acceleration brought on by gravity, and K_1 is the porous medium's permeability.. The suction velocity, velocity and thermal slip factors are defined as follows:

$$V(x,t) = V_0(1-\alpha t)^{-1/2}\ \ e^{x/2L}, N = N_1(1-\alpha t)^{1/2} e^{-x/2L}, E = E_1(1-\alpha t)^{1/2} e^{-x/2L}$$

where N_1 is the initial value of velocity slip factor and E_1 is the initial value of thermal slip factor while $N = E = 0$ indicates a no-slip condition.

According to Rosseland approximation [25], q_r is defined by the following formula:

$$q_r = -\frac{4\,\sigma^*}{3K^*}\frac{\partial}{\partial y}\,(T^4) \tag{5}$$

where σ^* and K^* are the Stefan-Boltzman constant and the absorption coefficient respectively. Expanding T^4 in a Taylor series around T_∞ and ignoring the second order and higher terms in $(T - T_\infty)$, we obtain

$$T^4 \cong 4T_\infty^3\, T - 3T_\infty^4$$

Then the equation (3) can be written as follows:

$$\frac{\partial T}{\partial t}+u\frac{\partial T}{\partial x}+v\frac{\partial T}{\partial y}=\frac{\kappa}{\rho\, C_p}\frac{\partial^2 T}{\partial y^2}+\frac{16\,\sigma^* T_\infty^3}{3\rho\, C_p K^*}\frac{\partial^2 T}{\partial y^2}+\frac{\sigma B^2}{\rho C_p}u^2+\frac{\mu}{\rho\, C_p}\left(\frac{\partial u}{\partial y}\right)^2+\frac{1}{\rho\, C_p}Q_0(T-T_\infty) \tag{6}$$

The following dimensionless variables are introduced in order to solve the momentum and energy equations (2) and (3):

$$\eta=\sqrt{\frac{U_0}{2\,\nu L\,(1-\alpha t)}}e^{x/2L}\,y\,,\qquad \psi=\sqrt{\frac{2\,L\,U_0\,\nu}{1-\alpha t}}e^{x/2L}\,f(\eta),\qquad T=T_\infty+\frac{T_0}{(1-\alpha t)^2}e^{x/2L}\;\theta(\eta)$$

Substituting the above variables into the equations (2)-(3), the subsequent equations are obtained as:

$$f'''+\,f\,f''-2\,f'^2-A\,e^{-X}\,(2f'+\eta\,f'')+\lambda\theta-(M+K)\,f'=0 \tag{7}$$

$$\left(1+\frac{4}{3}\,R\right)\theta''+\Pr(f\,\theta'-f'\,\theta)-e^{-X}A\Pr(4\theta+\eta\,\theta')+e^{-\frac{1}{2}X}H\Pr f'^2+e^{-\frac{1}{2}X}Ec\Pr f''^2+e^{-X}Q_H\Pr\theta=0 \tag{8}$$

with reduced boundary conditions:

$$f'(0)=1+S_f f''(0)\;\;,\qquad f(0)=S,\qquad \theta(0)=1+\boldsymbol{S}_t\,\theta'(0),\quad \text{at}\,\eta=0$$
$$f'(\infty)\to 0,\qquad \theta(\infty)\to 0\;\;\text{as}\;\eta\to\infty \tag{9}$$

where the prime denotes the differentiation w.r.t η. Also

$$Re_x=\frac{x\,U}{\nu},M=\frac{2L\sigma\,B_0^2}{\rho\,U_o},A=\frac{\alpha L}{U_o},\mathrm{X}=\frac{x}{L},K=\frac{2L\,\nu}{K_0U_0},\mathrm{Gr}=\frac{2g\beta(T_w-T_\infty)}{U^2},\lambda=\frac{Gr}{R_{e_x}^2},\mathrm{S}=\frac{V_0}{\sqrt{\frac{U_0\,\nu}{2L}}},\mathrm{R}=\frac{4\sigma^*T_\infty^3}{\kappa\,K^*},$$

$$H=M.Ec,Ec=\frac{U_0^2}{C_pT_0},Q_H=\frac{2LQ_0\,(1-\alpha t)}{\rho\,C_pU_o},\Pr=\frac{\rho\,C_p\nu}{\kappa},S_f=N_1\sqrt{\frac{U_0\,\nu}{2L}}\;and\;\boldsymbol{S}_t=E_1\sqrt{\frac{U_0}{2\,\nu L}}$$

are the local Reynolds number, magnetic parameter, unsteadiness parameter, dimensionless coordinate, porosity parameter, local Grashof number, mixed convection parameter, suction parameter, radiation parameter, joule heating parameter, Eckert number, heat generation ($Q_H > 0$) and absorption ($Q_H < 0$) parameter, Prandtl number, velocity and thermal slip parameter respectively. The co-efficient of skin-friction and Nusselt number are given by

$$C_f=\frac{2\,\tau_w}{\rho\,U^2}=\frac{2\,\mu\left(\frac{\partial u}{\partial y}\right)_{y=0}}{\rho\,U^2}=\sqrt{\frac{2x}{L}}\,(Re_x)^{-\frac{1}{2}}f''(0)\quad and \tag{10}$$

$$N_{u_x}=\frac{x\,q_w}{k(T_w-T_\infty)}=\frac{-xk\left(\frac{\partial T}{\partial y}\right)_{y=0}}{k(T_w-T_\infty)}=-\sqrt{\frac{x}{2L}}\;\sqrt{Re_x}\,\theta'(0) \tag{11}$$

3. METHODOLOGY

The non-linear ODEs (7) and (8), alongside conditions (9), are worked out numerically using MATLAB's bvp4c solver. This solver employs the three-stage Lobatto IIIa collocation method, which guarantees a solution that is C1-continuous and maintains fourth-order accuracy across the entire integration range. Prior to applying this method, the original equations are transformed into a first-order system of ODEs.

$$y_1=f,y_2=f',y_3=f'',y_4=\theta,y_5=\theta'$$

In MATLAB, a new set of variables is added as follows in order to find the numerical solution

$$y_2{}'=y_1$$
$$y_3{}'=y_2$$
$$y_3{}'=-y_1y_3+2y_2{}^2+A\,e^{-X}\,(2y_2+\eta\,y_3)-\lambda y_4+(M+K)y_2$$
$$y_4{}'=y_5$$

$$y_5{}' = \frac{1}{1+\frac{4}{3}R}\left[-\Pr(y_1y_5 - y_2y_4) + e^{-X}A\Pr(4y_4 + \eta\, y_5) - e^{-\frac{1}{2}X}H\Pr {y_2}^2 - e^{-\frac{1}{2}X}Ec\Pr {y_3}^2 - e^{-X}Q_H\Pr y_4\right]$$

with associated boundary conditions

$$y0(2) - 1 - S_f y0(3) = 0, y0(1) - S = 0, y0(4) - 1 - \boldsymbol{S}_t y0(5) = 0$$
$$yinf(2) = 0, yinf(4) = 0$$

4. RESULTS AND DISCUSSION

The resulting data reveal the effects of various non-dimensional governing parameters on the velocity and temperature profiles. These parameters include the mixed convection parameter (λ), magnetic parameter (M), unsteadiness parameter (A), porosity parameter (K), radiation parameter (R), joule heating parameter (H), Eckert number(Ec), heat generation/absorption parameter (Q_H), Prandtl number (Pr), suction/blowing parameter ($\boldsymbol{S}$), velocity slip parameter (S_f) and thermal slip parameter (S_t) on the velocity and temperature profiles. Table 1 displays the Nusselt number and Skin-friction co-efficient values for various parameters. For numerical computations, $X = 1.5, A = 0.1, M = 1, K = \lambda = H = 0.5, R = Ec = S = 0.2, Pr = 5,\ Q_H = S_t = 0.3, S_f = 0.05\ and\ \eta = 2$ are considered. These values are considered consistent across the study, except for the variations shown in the corresponding figures and tables.

Figures 1-6 are sketched to know the influences of $M, A, K, \lambda,\ S$ and S_f on velocity profile $(f'(\eta))$. Figure 1 describes how M influences $f'(\eta)$, showing a decrease in $f'(\eta)$ as M increases. This occurs because a stronger magnetic field M generates greater resistance forces, reducing $f'(\eta)$. In Figure 2, the impact of parameter A is shown, where $f'(\eta)$ increases with higher values of A. Figure 3 presents the effect of K on $f'(\eta)$, indicating a decrease in $f'(\eta)$ as K increases. This result can be explained through Darcy's law, which indicates that the presence of a porous medium decreases flow resistance. The influence of λ is depicted in Figure 4, where an increase in λ results in a higher fluid velocity. This is due to λ enhancing thermal buoyancy effects, which act as a favourable pressure gradient and accelerate fluid flow, thereby increasing the velocity boundary layer thickness. Figure 5 illustrates how the suction parameter S affects fluid velocity at the stretching sheet. Specifically, $f'(\eta)$ decreases with increasing suction $(S > 0)$ and increases with blowing $(S < 0)$.

Finally, Figure 6 shows the effect of S_f on $f'(\eta)$, revealing that $f'(\eta)$ decreases as S_f enhances.

Figures 7-18 elucidate the influences of $M, A, K, \lambda, S, S_f, R, Pr, Ec, H, Q_H$ and S_t on temperature profile, denoted as $\theta(\eta)$. Figure 7 demonstrates the effect of M on $\theta(\eta)$. It is observed that $\theta(\eta)$ increases with a rise within M. The effect of A on $\theta(\eta)$ is drawn in figure 8 which indicates that $\theta(\eta)$ also increases because A increases. Figure 9 shows that when K values grow, $\theta(\eta)$ rises as well. Figure 10 exhibits the influence of λ on $\theta(\eta)$. The fluid temperature reduces as λ enhances. Figure 11 shows the effect of S on $\theta(\eta)$. It is noted that $\theta(\eta)$ decreases with increasing suction parameter ($S > 0$) but it augments in consequence of blowing ($S < 0$). Figure 12 makes it clear that when S_f grows, so does $\theta(\eta)$. Figure 13 describes the influence of R on $\theta(\eta)$. We see that $\theta(\eta)$ increases because R increases suggesting that reducing thermal radiation can accelerate the cooling process. Figure 14 illustrates the influence of Pr on $\theta(\eta)$. We observe that when Pr accelerates, $\theta(\eta)$ diminishes. Figure 15 demonstrates the effect of Ec on $\theta(\eta)$. We notice that $\theta(\eta)$ enhances with the rise in Ec. The influence of H on $\theta(\eta)$ is portrayed in figure 16 which reveals that $\theta(\eta)$ also increases with the increasing values of H. The nature of $\theta(\eta)$ for various values of Q_H is presented in figure 17. An increase in heat generation ($Q_H > 0$) leads to a higher $\theta(\eta)$, whereas heat absorption $Q_H < 0$). results in a lower $\theta(\eta)$. Figure 18 depicts the variation of $\theta(\eta)$ against S_t. It is noted that when S_t increases, $\theta(\eta)$ falls. As S_t increases, less heat is transmitted from the sheet to the fluid, resulting in a drop in $\theta(\eta)$. Figures 19 and 20 illustrate the impacts of S, S_f and S_t on velocity and temperature gradients. Figure 19 shows how the velocity gradient $f''(0)$ varies with different suction values for various S_f levels. The graph indicates that the skin friction coefficient increases with higher values of S_f. Figure 20 presents the effect of S_t on the local temperature gradient against S. We become aware of that the Nusselt number decreases as S_t augments, reflecting a reduction in the local temperature gradient.

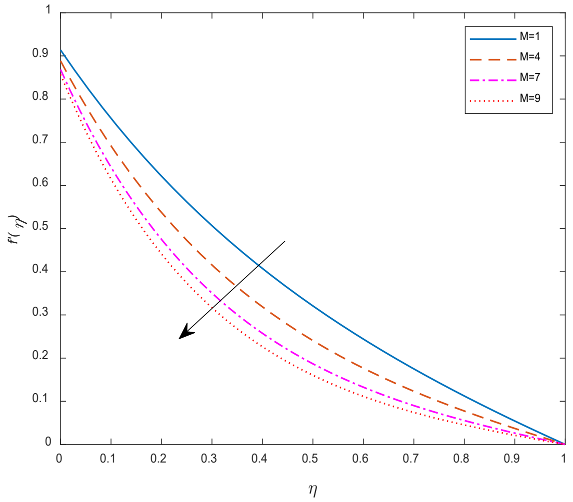

Figure 1. $f'(\eta)$ for M

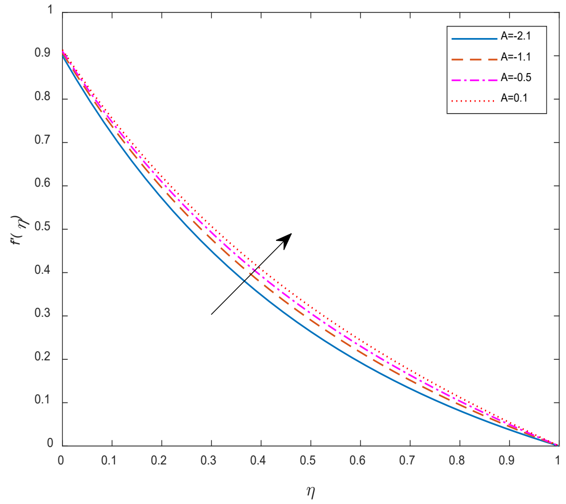

Figure 2. $f'(\eta)$ for A

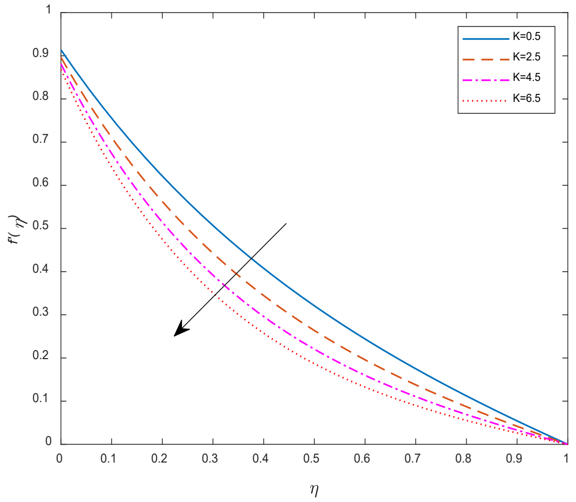

Figure 3. $\boldsymbol{f'(\eta)}$ **for** $\boldsymbol{K}$

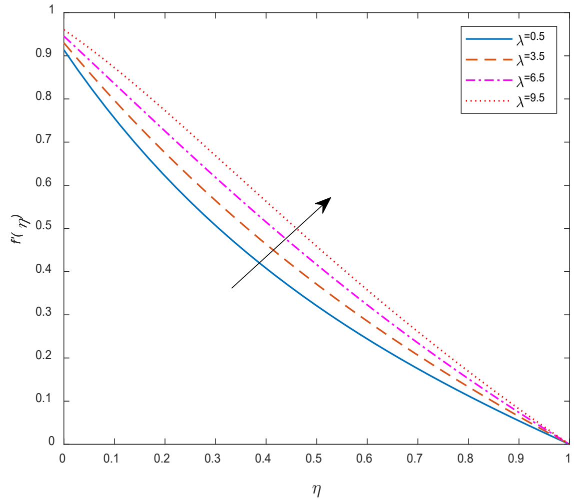

Figure 4. $\boldsymbol{f'(\eta)}$ **for** $\boldsymbol{\lambda}$

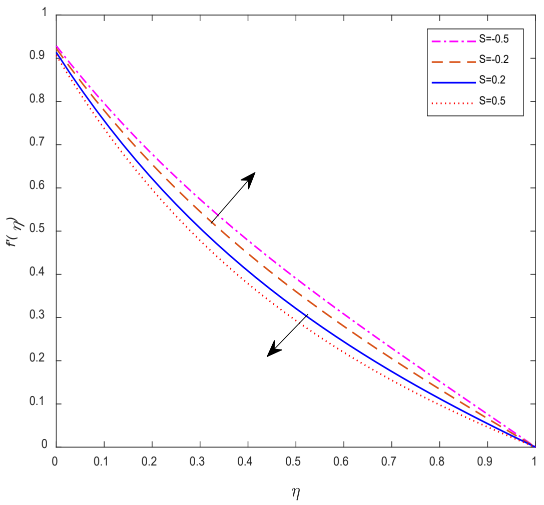

Figure 5. $f'(\eta)$ for S

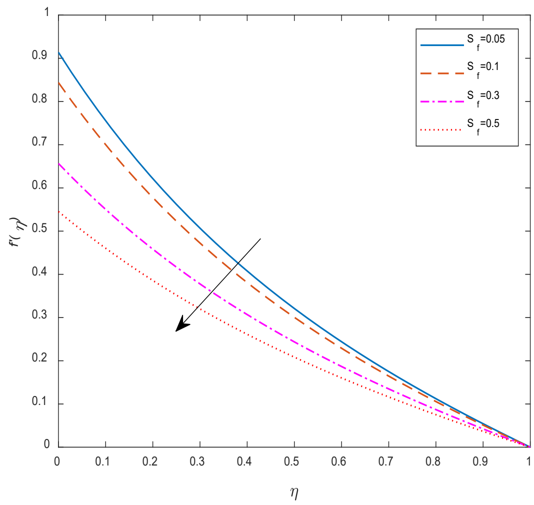

Figure 6. $f'(\eta)$ for S_f

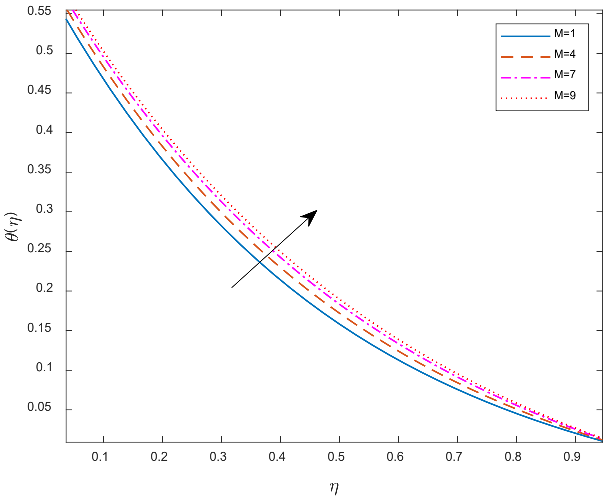

Figure 7. $\theta(\eta)$ for M

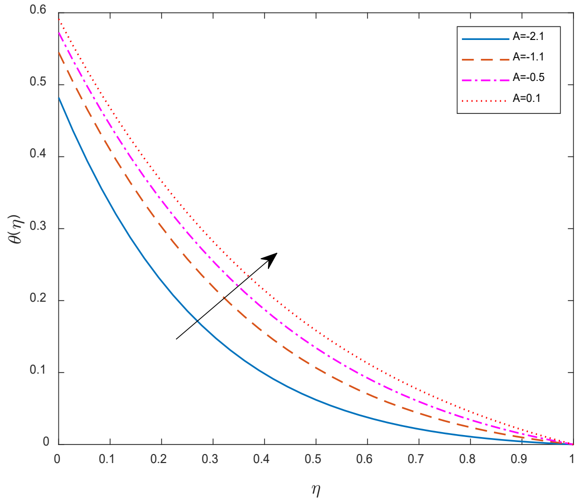

Figure 8. $\theta(\eta)$ for A

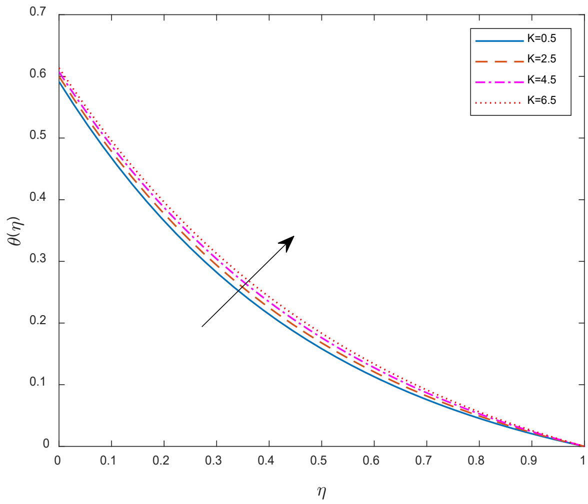

Figure 9. $\theta(\eta)$ for K

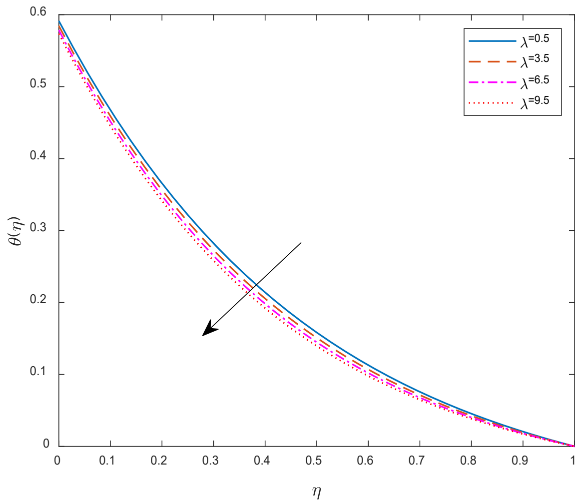

Figure 10. $\theta(\eta)$ for λ

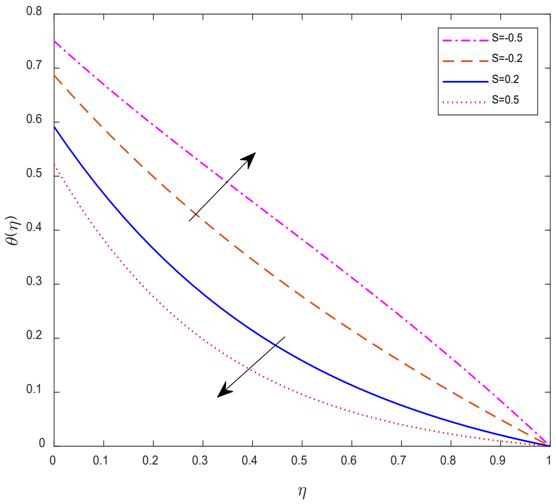

Figure 11. $\theta(\eta)$ for S

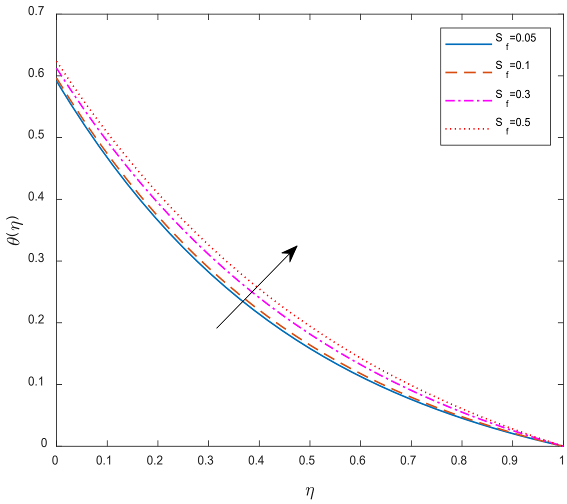

Figure 12. $\theta(\eta)$ for S_f

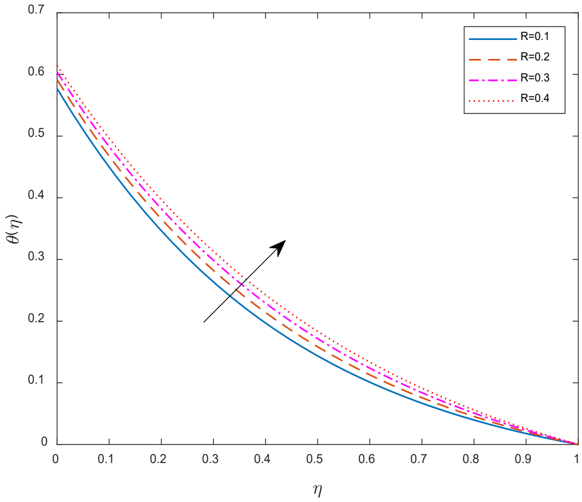

Figure 13. $\theta(\eta)$ for R

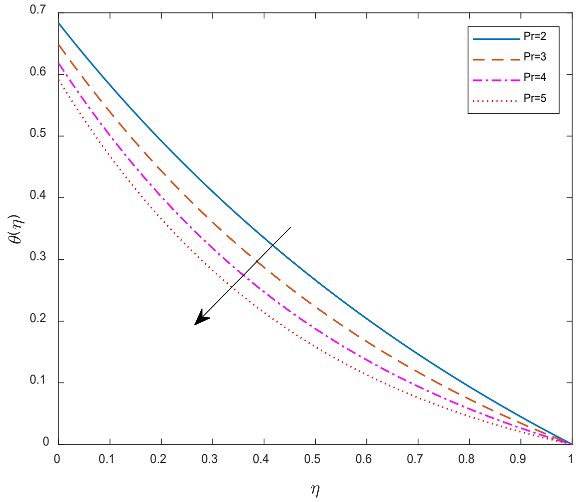

Figure 14. $\theta(\eta)$ for Pr

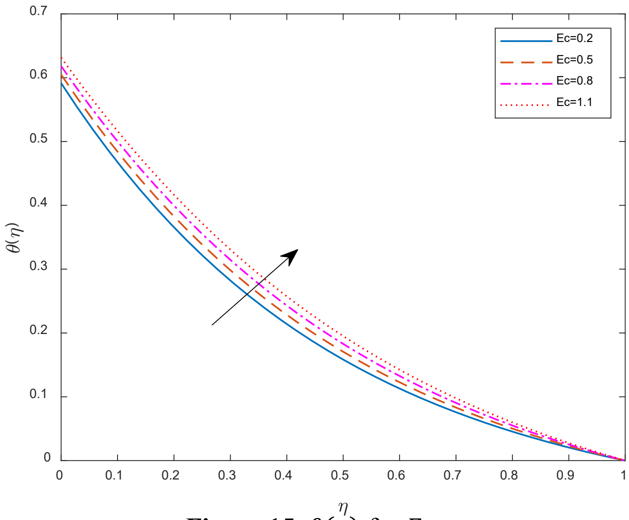

Figure 15. $\theta(\eta)$ for Ec

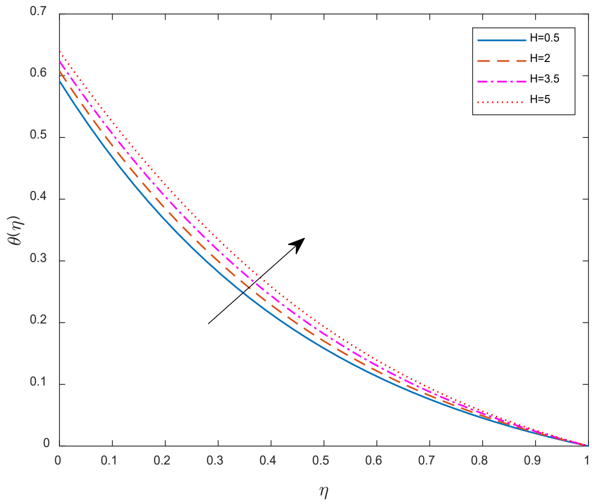

Figure 16. $\theta(\eta)$ for H

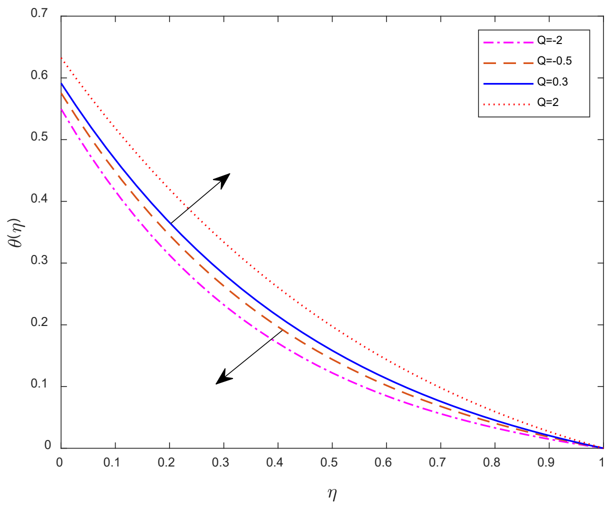

Figure 17. $\theta(\eta)$ for Q_H

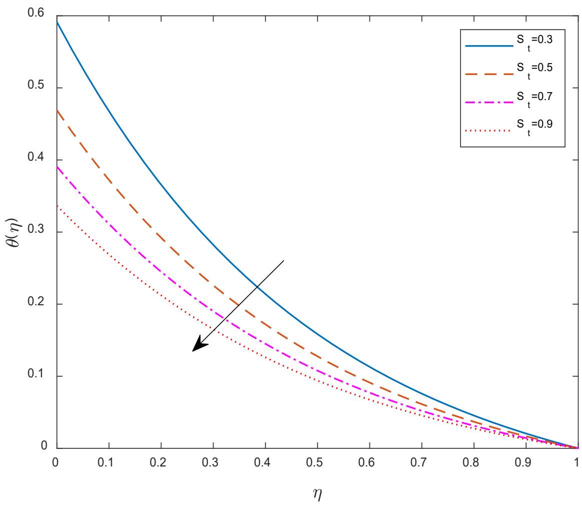

Figure 18. $\theta(\eta)$ for S_t

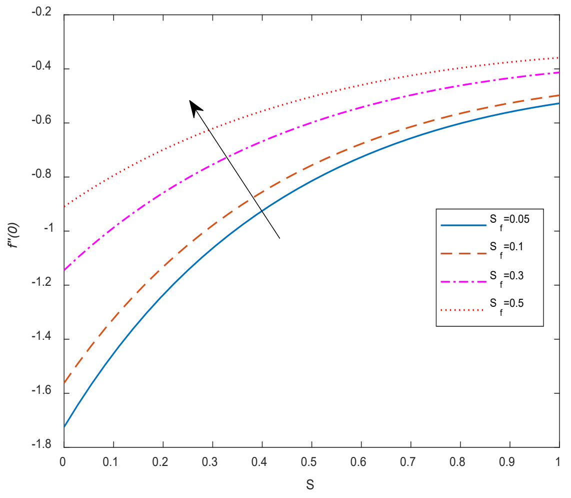

Figure 19. Velocity gradient for S_f against S

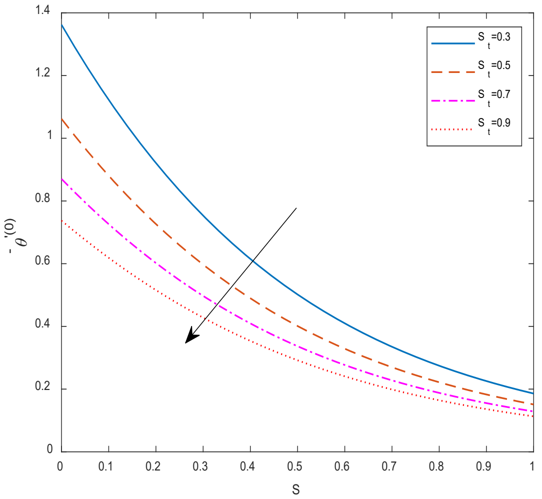

Figure 20. Temperature gradient for S_t against S

Table 1. Skin friction and Nusselt number for various values of important governing parameters

M	A	K	λ	S	S_f	Pr	R	H	Ec	Q	S_t	$f''(0)$	$-\theta'(0)$
1.0												-1.7248	1.3621
4.0												-2.2289	1.3212
7.0												-2.6303	1.2877
	-1.1											-1.8620	1.5171
	-0.5											-1.7897	1.4248
	0.1											-1.7248	1.3621
		2.5										-2.0748	1.3339
		4.5										-2.3719	1.3093
		6.5										-2.6303	1.2877
			3.5									-1.3989	1.3850
			6.5									-1.0899	1.4044
			9.5									-0.7944	1.4211
				-0.5								-1.4252	0.8332
				-0.2								-1.5481	1.0443
				0.5								-1.8642	1.5944
					0.1							-1.5622	1.3451
					0.3							-1.1448	1.2919
					0.5							-0.9094	1.2543
						2.0						-1.7053	1.0562
						3.0						-1.7129	1.1717
						4.0						-1.7193	1.2729
							0.1					-1.7276	1.4098
							0.3					-1.7223	1.3210
							0.4					-1.7201	1.2851
								2.0				-1.7221	1.3089
								3.5				-1.7193	1.2555
								5.0				-1.7166	1.2021
									0.5			-1.7223	1.3174
									0.8			-1.7198	1.2729
									1.1			-1.7173	1.2286
										-2.0		-1.7325	1.5012
										-0.5		-1.7278	1.4153
										2.0		-1.7169	1.2249
											0.5	-1.7361	1.0620
											0.7	-1.7434	0.8703
											0.9	-1.7485	0.7373

From the Table 1, we see that skin friction coefficient rises owing to increase of $A, \lambda, S_f, R, H, Ec, Q_H$ while it reduces because of increase of $M, , K, S, Pr$ and S_t. Conversely, the Nusselt number is observed to increase with the enhancement of λ, S and Pr. However, it decreases with the rise in $A, M, K, S_f, R, H, Ec, Q_H$ and S_t.

5. CONCLUSIONS

The numerical analysis examines the outcomes of double slip on MHD mixed convective unsteady flow over an ESS in a porous medium. The results, depicted graphically and in tables, highlight the impact of various parameters on coefficient of skin friction, velocity $f'(\eta)$, temperature $\theta(\eta)$, and Nusselt number. The key features are as follows:

- Increasing the thermal slip factor S_f reduces fluid velocity $(f'(\eta)$ and the Nusselt number but increases $\theta(\eta)$ and the skin friction coefficient. Conversely, S_t reduces $\theta(\eta)$.
- Parameters M and K lower $f'(\eta)$ while rising $\theta(\eta)$.
- Mixed convection parameter (λ) increases the $f'(\eta)$ while decreasing $\theta(\eta)$.
- Higher values of Ec, R and H increase $\theta(\eta)$.
- An increase in Pr accelerates Nusselt number but lowers temperature profile and skin friction
- Larger A accelerates both $f'(\eta)$ and $\theta(\eta)$.
- Suction increases, and blowing decreases $f'(\eta)$ and $\theta(\eta)$.
- Nusselt number and the coefficient of skin friction decrease with higher S_t.

ACKNOWLEDGEMENTS

Institution(s)
All the authors would like to express their gratitude to Port City International University for the support/ facilities.

Fund
This study was not supported by any grants from funding bodies in the public, private, or not-for-profit sector.

Individual Assistant
NA

DECLARATION OF ORIGINALITY

The authors declare no conflict of interest to report regarding this study conducted.

REFERENCES

[1] Isa SS, Arifin NM, Nazar R, Bachok N, Ali FM. The effect of convective boundary condition on MHD mixed convection boundary layer flow over an exponentially stretching vertical sheet. In. Journal of Physics: Conference Series 2017 Dec 1 (Vol. 949, No. 1, p. 012016). IOP Publishing.

[2] Shateyi S, Marewo GT. Numerical solution of mixed convection flow of an MHD Jeffery fluid over an exponentially stretching sheet in the presence of thermal radiation and chemical reaction. Open Physics. 2018 May 24;16(1):249-59.

[3] Rehman A, Salleh Z. Approximate analytical analysis of unsteady MHD mixed flow of non-Newtonian hybrid nanofluid over a stretching surface. Fluids. 2021 Apr 1;6(4):138.

[4] Kanafiah SF, Kasim AR, Zokri SM, Al Sharifi HA. Mixed convection flow of Brinkman fluid with convective boundary condition at lower stagnation point of horizontal circular cylinder. Data Analytics and Applied Mathematics (DAAM). 2021:01-10.

[5] Yahaya RI, Arifin NM, Pop I, Ali FM, Isa SS. Dual solutions of unsteady mixed convection hybrid nanofluid flow past a vertical Riga plate with radiation effect. Mathematics. 2023 Jan 1;11(1):215.

[6] Jha BK, Samaila G. Thermal radiation effect on boundary layer over a flat plate having convective surface boundary condition. SN Applied Sciences. 2020 Mar; 2(3):381.

[7] Hakeem AA, Kalaivanan R, Ganesh NV, Ganga B. Effect of partial slip on hydromagnetic flow over a porous stretching sheet with non-uniform heat source/sink, thermal radiation and wall mass transfer. Ain Shams Engineering Journal. 2014 Sep 1; 5(3):913-22.

[8] Ishak A. MHD boundary layer flow due to an exponentially stretching sheet with radiation effect. Sains Malaysiana. 2011 Apr 1; 40(4):391-5.

[9] Sharma K, Gupta S. Analytical study of MHD boundary layer flow and heat transfer towards a porous exponentially stretching sheet in presence of thermal radiation. International Journal of Advances in Applied Mathematics and Mechanics. 2016;4(1):1-0.

[10] Omar NF, Ismail Z, Jusoh R, Samah RA, Osman HI, Mohamad AQ. Mixed convection casson fluids with the effects of porosity and radiation. Data Analytics and Applied Mathematics (DAAM). 2022 Sep 30:18-24.

[11] Khan MS, Karim I, Ali LE, Islam A. Unsteady MHD free convection boundary-layer flow of a nanofluid along a stretching sheet with thermal radiation and viscous dissipation effects. International nano letters. 2012 Dec; 2:1-9.

[12] Srinivasacharya D, Jagadeeshwar P. Effect of Joule heating on the flow over an exponentially stretching sheet with convective thermal condition. Mathematical Sciences. 2019 Sep; 13:201-11.

[13] Alinejad J, Samarbakhsh S. Viscous flow over nonlinearly stretching sheet with effects of viscous dissipation. Journal of Applied Mathematics. 2012;2012(1):587834.

[14] Dessie H, Kishan N. MHD effects on heat transfer over stretching sheet embedded in porous medium with variable viscosity, viscous dissipation and heat source/sink. Ain shams engineering journal. 2014 Sep 1;5(3):967-77.

[15] Patil PM, Latha DN, Roy S, Momoniat E. Double diffusive mixed convection flow from a vertical exponentially stretching surface in presence of the viscous dissipation. International Journal of Heat and Mass Transfer. 2017 Sep 1; 112:758-66.

[16] Shahzad F, Sagheer M, Hussain S. Numerical simulation of magnetohydrodynamic Jeffrey nanofluid flow and heat transfer over a stretching sheet considering Joule heating and viscous dissipation. AIP Advances. 2018 Jun 1;8(6).

[17] Mohamed MK, Hussanan A, Alkasasbeh HT, Widodo B, Salleh MZ. Boundary layer flow on permeable flat surface in Ag-Al_2O_3/water hybrid nanofluid with viscous dissipation. Data Analytics and Applied Mathematics (DAAM). 2021 Jun 29:11-8.

[18] Mukhopadhyay S, Mandal IC. Magnetohydrodynamic (MHD) mixed convection slip flow and heat transfer over a vertical porous plate. Engineering Science and Technology, an International Journal. 2015 Mar 1;18(1):98-105.

[19] Mukhopadhyay S. Analysis of boundary layer flow over a porous nonlinearly stretching sheet with partial slip at the boundary. Alexandria Engineering Journal. 2013 Dec 1;52(4):563-9.

[20] Ramzan M, Dawar A, Saeed A, Kumam P, Watthayu W, Kumam W. Heat transfer analysis of the mixed convective flow of magnetohydrodynamic hybrid nanofluid past a stretching sheet with velocity and thermal slip conditions. Plos one. 2021 Dec 14;16(12):e0260854.

[21] Islam MA, Ali MY, Gani SM. Unsteady heat and mass transfer slip flow over an exponentially permeable stretching sheet. Journal of Scientific Research. 2022 May 6;14(2):443-57.

[22] Islam MA, Ali MY, Akter R, Gani SO. Unsteady Mixed Convection Slip Flow around a Stretching Sheet in Porous Medium. Journal of Applied Mathematics and Physics. 2022 Sep 30;10(10):3016-36.

[23] Akter R, Islam MA. Unsteady Williamson Fluid Flow Over Exponentially Stretching Sheet in the presence of Non-Uniform Heat Generation or Absorption and Inclined Magnetic Field. Journal of Scientific Research. 2023 Aug 13;15(3):621-36.

[24] Mukhopadhyay S. Slip effects on MHD boundary layer flow over an exponentially stretching sheet with suction/blowing and thermal radiation. Ain Shams Engineering Journal. 2013 Sep 1;4(3):485-91.

[25] Brewster MQ. Thermal radiative transfer and properties. John Wiley & Sons; 1992 Apr 16.